Metabolism Clinical and Experimental 98 (2019) 95–103

Contents lists available at ScienceDirect

Metabolism Clinical and Experimental

journal homepage: www.metabolismjournal.com

LC3 promotes the nuclear translocation of the vitamin D receptor and decreases fibrogenic gene expression in proximal renal tubules

Aimei Li [a], Hao Zhang [a], Hailong Han [b], Wei Zhang [a], Shikun Yang [a], Zhijun Huang [c], Jieqiong Tan [b], Bin Yi [a,*]

[a] Department of Nephrology, The Third Xiangya Hospital, Central South University, Changsha, Hunan 410013, China
[b] Center for Medical Genetics, School of Life Sciences, Central South University, Changsha, Hunan 410008, China
[c] Center for Clinical Pharmacology, the Third Xiangya Hospital, Central South University, Changsha, Hunan 410013, China

ARTICLE INFO

Article history:
Received 4 January 2019
Accepted 14 June 2019

Keywords:
LC3
Vitamin D receptor
Nuclear translocation

ABSTRACT

Diabetic nephropathy (DN) is a major cause of end-stage renal disease (ESRD). Vitamin D receptor (VDR) belongs to the nuclear receptor superfamily and exerts a renoprotective effect through inhibiting fibrosis. Microtubule-associated protein 1 light chain 3 (LC3), a key regulator of autophagy, is abundant in the nucleus, although its primary function is in the cytoplasm. The role of nuclear LC3 and the mechanism by which LC3 shuttles between the cytoplasm and nucleoplasm has not been fully elucidated. We found that LC3 binds to VDR in an LC3-interacting region (LIR)-independent manner and promotes the nuclear translocation of VDR. Further study indicated that LC3 promotes the formation of the VDR:retinoid X receptor (RXR) heterodimer and inhibits fibrogenic genes expression in HK-2 cells induced by high glucose. Our result demonstrates that LC3 is a negative regulator of high glucose-induced fibrogenic genes expression through its ability to promote VDR signaling.

1. Introduction

Diabetic nephropathy (DN) is an important complication of diabetes mellitus (DM) and is a major factor associated with increased mortality and morbidity in diabetic patients, mainly due to cardiovascular disease [1]. Due to the increasing incidence of diabetes, DN has become the leading cause of end-stage renal disease (ESRD) worldwide. The pathologic changes of DN are characterized initially by glomerular and tubuloepithelial hypertrophy, glomerular and tubular basement membrane thickening, followed by hyperfiltration, albuminuria, glomerulosclerosis, and tubulointerstitial fibrosis, leading eventually to ESRD [2].

Vitamin D receptor (VDR) is a ligand-activated transcription factor that belongs to the nuclear receptor superfamily. After being activated, VDR forms heterodimer with retinoid X receptor (RXR) and enters the nucleus, which regulates target gene transcription by interacting with the promoters of these genes [3]. Studies have demonstrated that the expression of VDR in chronic kidney disease, including DN, is decreased [4,5]; this decrease is believed to contribute to the pathogenesis of kidney disease. VDR can exert a renoprotective effect through multiple mechanisms, such as inhibiting inflammation, preventing fibrosis and inhibiting the renin-angiotensin (RAS) system [6].

Microtubule-associated protein 1 light chain 3 (LC3), which is a key regulator of autophagy, is a basic protein with arginine-rich sequences [7]. The LC3 subfamily comprises LC3A, LC3B and LC3C, and all associate with autophagosomes [8]. Although LC3 is mainly involved in the autophagic process, studies have shown that it also participates in other cellular activities [9–13]. LC3 is abundant in the nucleus, but its primary function is in the cytoplasm, where autophagosomes and autolysosomes are formed. Nuclear LC3 has been considered as a reserve for the cytoplasmic pool, shifting to the cytosol after nutrient deprivation and subsequently being transformed to its lipidated form and being incorporated into autophagic membranes [14]. However, the role of nuclear LC3 is not yet clear. In our study, we demonstrated that LC3 interacted with VDR and promoted the nuclear translocation of VDR and the formation of the VDR:RXR heterodimer, thus regulating the expression of fibrotic genes.

2. Experimental procedures

2.1. Reagents, antibodies and plasmids

DMEM was from HyClone (SH30022.01, SH30023.01). Fetal bovine serum was from Gibco (16000-044). The complete protease cocktail was from Roche. Lipofectamine 2000 was from Invitrogen. Protein G agarose was from KPL (223-51-01). Mouse anti-Flag (M2) affinity gels were from Sigma-Aldrich (A2220). The following antibodies were

Abbreviations: DN, diabetic nephropathy; ESRD, end-stage renal disease; VDR, vitamin D receptor; LC3, microtubule-associated protein 1 light chain 3; LIR, LC3-interacting region; RXR, retinoid X receptor; AIM, Atg8-interacting motif.

* Corresponding author at: Department of Nephrology, The Third Xiangya Hospital, Central South University, 138 Tongzipo Road, Changsha 410013, Hunan, China.
E-mail address: yibin_yb@163.com (B. Yi).

https://doi.org/10.1016/j.metabol.2019.06.008
0026-0495/

used: anti-VDR (Santa Cruz Biotechnology, SC-13133); anti-LC3A (Cell Signaling, 4599); anti-LC3B (Cell Signaling, 2775); anti-LC3C (Cell Signaling, 14736); anti-histone H3 (Cell Signaling, 14269); anti-Flag tag (Cell Signaling, 2368); anti-p62 (Sigma-Aldrich, P0067); and anti-RXRα (Abcam, ab125001). All secondary antibodies were from Jackson ImmunoResearch Laboratories. cDNA encoding LC3 was PCR-generated and subcloned into pEGFP-C1 (Clontech, 6085-1) to express GFP-LC3. VDR-Flag was constructed by GeneChem through subcloning a

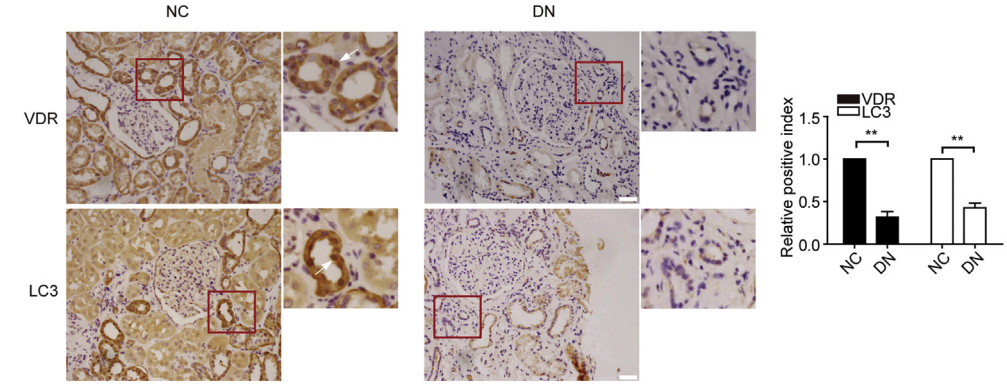

A) Patient tissues

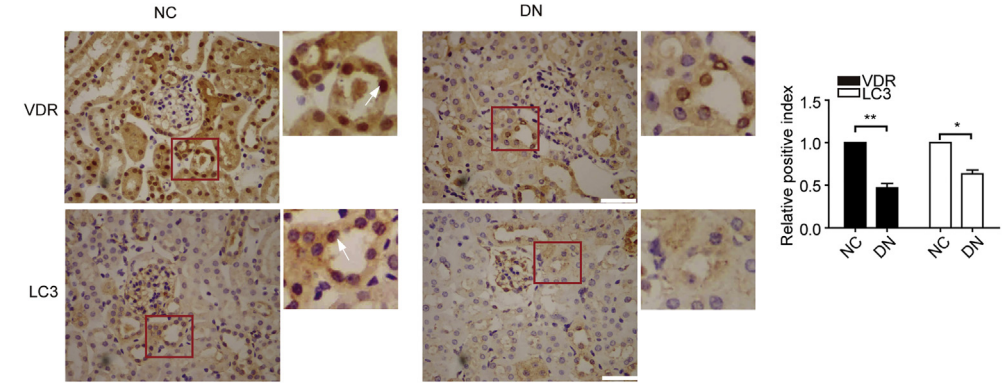

B) Mouse tissues

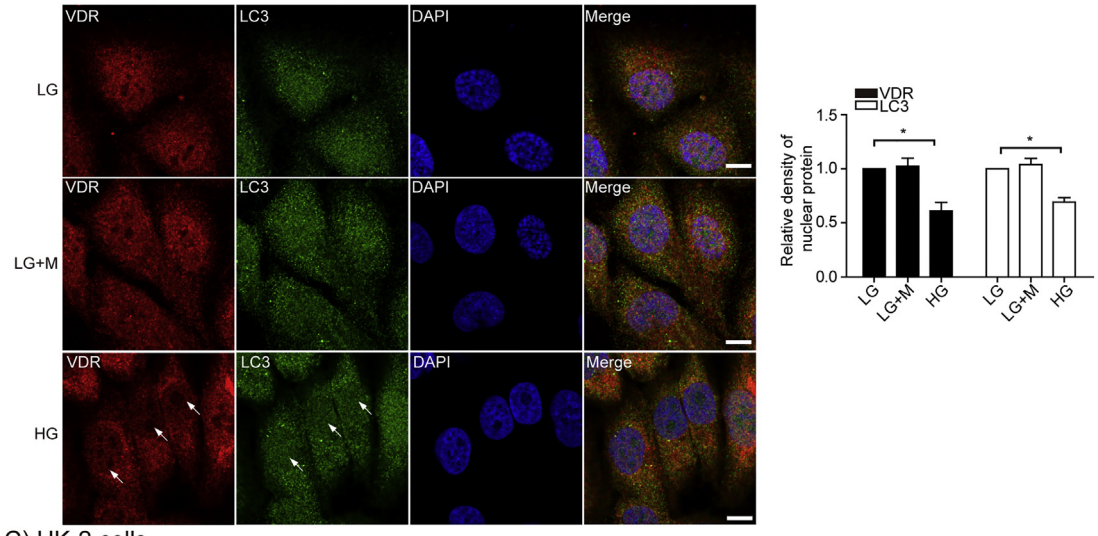

C) HK-2 cells

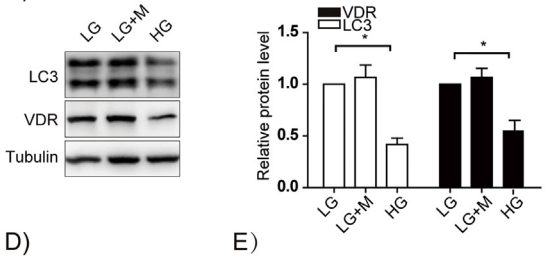

D) E)

sequence encoding the human VDR into GV141. GV141 (negative control plasmid) was provided by GeneChem. All plasmids were confirmed by sequencing.

2.2. Patients and animal tissue samples

Kidney biopsy samples from type II DM (T2DM) patients pathologically diagnosed with DN by percutaneous renal biopsy and from age- and gender-matched nondiabetic patients who underwent renal resection because of renal carcinoma (n = 3, NC group) were obtained from our previous study [4]. Eight-week-old male C57BL/6 mice were purchased from the Model Animal Research Center of Nanjing University. For DM induction, mice received intraperitoneal (i.p.) injections of either sodium citrate (pH 4.5, NC group) or 50 mg/kg streptozocin (STZ) (dissolved in sodium citrate, pH 4.5, DN group) for 5 consecutive days. One week later, mice with a casual blood glucose level above 16.7 mmol/L were used for the subsequent experiments. Kidneys were harvested 12 weeks after diabetes was induced. Sagittal kidney sections were fixed via the ventricular perfusion of 4% paraformaldehyde and embedded in paraffin. This study adhered to the Declaration of Helsinki. Ethical approval was obtained from the Third Xiangya Hospital of Central South University, and the patients were provided informed consent.

2.3. Cell culture and transfection

HEK293 cells and HK-2 cells were from the American Type Culture Collection (ATCC). HEK293 p62 knockout (KO) cells and HK-2 VDR KO cells were generated by using the CRISPR/Cas9 system. The sgRNA sequence for p62 KO is 5′-CGGCTTCCGCCTCAGGCTCG-3′, and the sgRNA sequence for VDR KO is 5′-ACGTTCCGGTCAAAGT CTCC-3′. HEK293 cells were cultured in DMEM with high glucose supplemented with 10% fetal bovine serum, 100 U/mL penicillin and 100 μg/mL streptomycin. HK-2 cells were cultured in DMEM with F12 (1:1) supplemented with 10% fetal bovine serum, 100 U/mL penicillin and 100 μg/mL streptomycin. Cells were incubated in a humidified incubator with 5% CO_2 at 37 °C. Cells were serum-starved overnight before treatment with low D-glucose (5 mM, LG), mannitol (25 mM mannitol + 5 mM D-glucose, LG + M) or high D-glucose (30 mM, HG) [15,16]. Transient transfections were performed using Lipofectamine 2000 according to the manufacturer's instructions (Invitrogen). Cells were harvested 24–48 h after transfection for the associated experiments.

2.4. RNAi

Small interfering RNA (siRNA) transfection was performed with 20 nM siRNA using Lipofectamine 3000 according to the manufacturer's instructions (Invitrogen). Cells were harvested 72 h after transfection. The siRNAs targeted the following sequences [17,18]: LC3A (5′-GGCT TCCTCTATATGGTCTACGCCT-3′), LC3B (5′-GCCUGUGUUGUUACGGAAA TT-3′), and LC3C (5′-GCTTGGCAATCAGACAAGAGGAAGT-3′). The siRNA 5′-TGGTTTTACATGTCGACTAA-3′ was used as the negative control (referred to as siRNA control).

2.5. Subcellular protein fractionation

Subcellular protein fractionation was performed according to the instructions for NE-PER nuclear and cytoplasmic extraction reagents (Thermo Scientific™). Briefly, HK-2 cells were washed with PBS, and ice-cold CER I was then added to the cell pellet. The tube was vortexed vigorously for 15 s and incubated for 10 min. Ice-cold CER II was added to the tube, vortexed, and centrifuged at 16000 ×*g* for 5 min at 4 °C. The supernatant was saved for analysis of cytoplasmic proteins, and the cell pellet was further resuspended in ice-cold NER. The sample was vortexed for 15 s, then placed on ice, and then for 15 s every 10 min for a total of 40 min. The sample was then centrifuged at 16000 ×*g* for 10 min at 4 °C. The levels of nuclear proteins in the supernatant were assessed using Western blotting. β-Actin and histone H3 were used as the cytoplasmic and nuclear markers, respectively.

2.6. Western blotting

Total protein was collected as previously described [19]. Protein concentrations were measured using a BCA protein assay kit (Pierce). Ten to 30 μg of total protein, cytoplasmic protein or nuclear protein was separated by SDS-polyacrylamide gel electrophoresis (PAGE) and electrotransferred to PVDF membranes (Millipore). The resulting membranes were blocked with PBST containing 5% nonfat milk for 1 h before incubation with primary antibodies at 4 °C overnight. After being washed three times with PBST, the membranes were further incubated with HRP-conjugated goat anti-mouse or anti-rabbit IgG at room temperature (RT) for 1 h. Finally, protein expression was measured using chemiluminescent staining reagent kits (SuperSignal West Femto) and images of the immunoreaction were captured using Image Scanner. The band intensities in the images were quantified with ImageJ software.

2.7. Coimmunoprecipitation (Co-IP)

Cells were rinsed once with ice-cold PBS and lysed in co-IP buffer (10 mM HEPES (pH 7.5), 142.5 mM KCl, 5 mM $MgCl_2$, 1 mM EDTA, 1% Triton X-100, and 10% glycerol) supplemented with protease inhibitors for 15 min at 4 °C. Cells were scraped off into clean 1.5 mL tubes and incubated with rotation for 1 h at 4 °C. The lysates were centrifuged at 13,000 rpm for 15 min at 4 °C, and the supernatant was immediately transferred to new tubes. Total protein or subcellular protein was quantified with a BCA assay, and the protein was diluted to 1 μg/μL in the co-IP buffer. IP was performed by incubation with either an anti-Flag M2 affinity gel or with corresponding antibodies and protein G on a rotating shaker at 4 °C overnight for 12 h. The samples were centrifuged at 14,000 ×*g* for 5 min, and the beads were retained and washed with cold PBS 5 times. Proteins bound to the beads were eluted with 40 μL of SDS-PAGE sample buffer and heated to 95 °C for 10 min. The supernatant was collected for subsequent Western blotting.

2.8. Immunofluorescence staining

HK-2 cells were fixed in 4% paraformaldehyde in PBS for 10 min at RT after being transfected with pEGFP-C1 or GFP-LC3 and were then

Fig. 1. High glucose suppresses the expression of nuclear VDR and LC3 in proximal renal tubules. (A) Immunohistochemical staining of VDR and LC3 proteins in normal renal tissues from nondiabetic kidneys (NC) and renal biopsies from T2DM patients with diabetic nephropathy (DN). VDR- or LC3-positive cells are stained brown, and nuclei are stained blue. Scale bar, 50 μm. The white arrows indicate examples of VDR- or LC3-positive cells. $^{**}P < 0.01$. (B) Immunohistochemical staining of VDR and LC3 proteins in normal renal tissues from control mice (NC) and mice with diabetic nephropathy (DN). Scale bar, 50 μm. The white arrows indicate examples of VDR- or LC3-positive cells. $^{*}P < 0.05$, $^{**}P < 0.01$. (C) Immunofluorescence staining of VDR (red) and LC3 (green) in HK-2 cells treated with low glucose (LG, 5 mM), mannitol (25 mM mannitol + 5 mM D-glucose, LG + M) or high glucose (HG, 30 mM) for 2 days. DAPI (blue) was used to stain nuclei. At least 10 microscopic fields were assessed in each experiment. The images are representative of three independent experiments. Scale bar, 10 μm. The white arrows indicate decreased expression of nuclear VDR or LC3. $^{*}P < 0.05$. (D) Expression of the VDR and LC3 in HK-2 cells treated with LG, LG + M or HG for 2 days. Tubulin was used as the loading control. (E) Quantitative analysis of the data in (D) by ImageJ software based on three independent experiments. $^{*}P < 0.05$.

permeabilized with 0.1% Triton X-100 in PBS for a further 10 min. After the cells were blocked in bovine serum albumin in PBS for 1 h, they were incubated with a human VDR (1:50) or LC3 (1:100) antibody at RT for 1 h. After being washed in PBST, the cells were incubated with an Alexa Fluor-conjugated goat anti-mouse or goat anti-rabbit secondary antibody for 1 h at RT. The cells were then stained with DAPI to visualize nuclei. Confocal microscopy was performed using a Leica TCS SP laser scanning microscope (Leica Microsystems, Exton, Pa.) fitted with a 100× Leica objective (Planaprochromatic; 1.4 numerical aperture) and connected to Leica image software.

2.9. Immunohistochemical staining

The VDR and LC3 levels in the formalin-fixed, paraffin-embedded tissues were evaluated using immunohistochemical staining. Briefly, the tissue sections (5 μm thickness) were deparaffinized and rehydrated, and microwave antigen retrieval was conducted in citrate buffer. After cooling, endogenous peroxidase was blocked with 3% hydrogen peroxidase for 10 min at RT. Then, the slides were blocked with 5% bull serum albumin for 1 h at RT and incubated overnight at 4 °C with primary antibodies against VDR (1:100) or LC3 (1:100). After being washed in PBS, the sections were incubated with the appropriate secondary antibody for 1 h at RT. After subsequent washes with PBS, DAB was applied for visualization of the indicated proteins, followed by counterstaining with hematoxylin to identify cell nuclei.

2.10. Real-time RT-PCR

HK-2 cells were incubated with LG, LG + M, or HG for 24 h or 72 h. Total RNA was extracted using TRIzol reagent (Invitrogen). cDNA was synthesized using the reverse transcription kit ReverTra Ace qPCR RT Kit (Thermo Scientific™) according to the manufacturer's instruction. Real-time quantitative PCR analysis was performed using SYBR Green PCR Master Mix (Thermo Scientific™) on an Applied Biosystems 7300 Sequence Detection System. PCR primers were designed using Oligo 6.0 software and synthesized by Shanghai Sangon. PCR was performed with oligonucleotide primers (R&D Systems) specifically designed to amplify VDR and genes implicated in renal fibrosis [6]: VDR (forward primer: 5′-CCAAGACTACAAGTACCGCG-3′ and reverse primer: 5′-TCAGCTTCTTCAGTCCCACC-3′), COL1A1 (forward primer: 5′-CAAGAG GCATGTCTGGTTCG-3′ and reverse primer: 5′-TAGGTGATGTTCTGGG AGGC-3′) and CTGF (forward primer: 5′-TACCAATGACAACGCCTCCT-3′ and reverse primer: 5′-TGGGAGTACGGATGCACTTT-3′). The relative amounts of mRNA were expressed as $2^{-\Delta\Delta CT}$ values.

2.11. Statistical analysis

Data were analyzed using SPSS 16.0 statistical software and expressed as the means ± standard deviations (SDs). Student's *t*-test was used to analyze the differences between groups with or without treatment. $P < 0.05$ was considered statistically significant.

3. Results

3.1. HG suppresses the expression of nuclear VDR and LC3 in proximal renal tubules

In the previous study, we found VDR protein was decreased in the tubular epithelial cells in renal biopsies from T2DM patients, compared with control. Next, we detected the proximal renal tubules expression of VDR and LC3 in renal tissues from DN patients and DN mouse models by immunohistochemical staining. The clinical characteristics of the study participants were shown in Table S1. 12 weeks after diabetes was induced, the diabetic mice had lower body weight and higher blood glucose than NC group (Fig. S1). VDR and LC3 were localized mostly in the nuclei of proximal renal tubular epithelial cells in normal renal tissues. However, the nuclear levels of VDR and LC3 were appreciably decreased in proximal renal tubular epithelial cells from DN patients (Fig. 1A) and DN mice (Fig. 1B). To confirm the effect of HG on the expression of VDR and LC3, we treated HK-2 cells with HG (30 mM) or controls for 2 days. Immunofluorescence results showed that the expression of nuclear VDR and LC3 were decreased (Fig. 1C) in the presence of HG, consistent with the in vivo results. Meanwhile, HG decreased the protein expression of VDR and LC3 in HK-2 cells (Fig. 1D–E).

3.2. LC3 promotes the nuclear translocation of VDR

To investigate the role of LC3 in the redistribution of VDR, we silenced the expression of LC3 subfamily members (LC3A, LC3B and LC3C) or overexpressed LC3 in HK-2 cells. Western blot analysis showed lower nuclear VDR and higher cytoplasmic VDR levels in LC3 knockdown cells than control cells (Fig. 2A–B). Conversely, in cells with LC3 overexpression, the expression of VDR was higher in

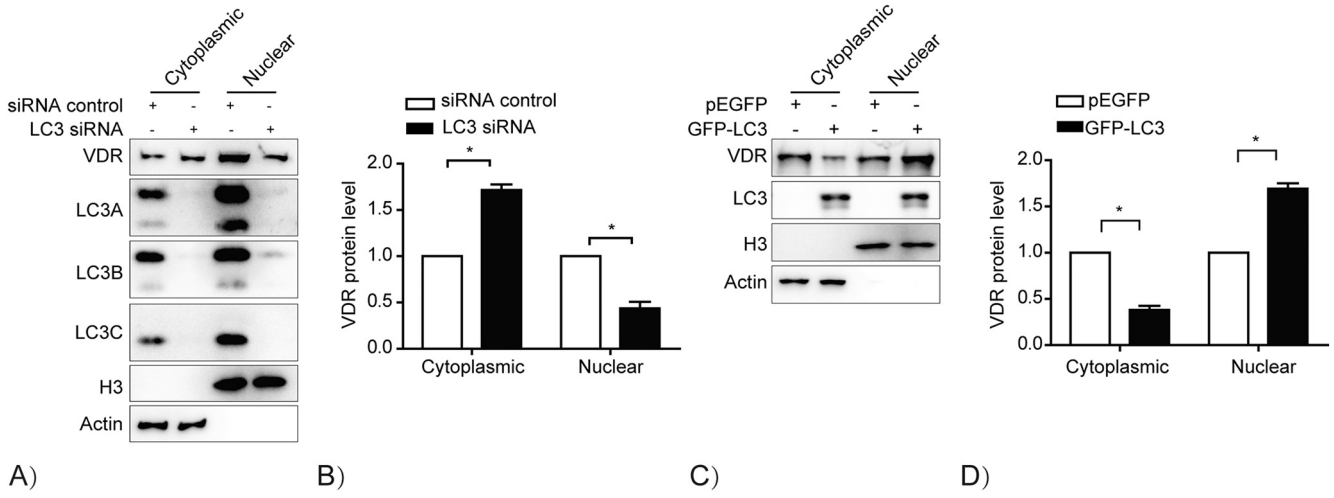

Fig. 2. LC3 promotes the nuclear translocation of VDR. (A) Western blot analysis of cytoplasmic and nuclear VDR protein levels at 72 h post transfection with control siRNA or LC3 siRNA. β-Actin (Actin) was used as the internal control for the cytoplasmic portion. H3 was used as the internal control for the nuclear portion. n = 3; a representative image is shown. (B) Quantitative analysis of the data in (A) by ImageJ software based on three independent experiments. *$P < 0.05$. (C) Western blot analysis of cytoplasmic and nuclear VDR protein levels at 24 h post transfection with pEGFP-C1 or GFP-LC3. Actin was used as the internal control for the cytoplasmic portion. H3 was used as the internal control for the nuclear portion. n = 3; a representative image is shown. (D) Quantitative analysis of the data in (C) by ImageJ software based on three independent experiments. *$P < 0.05$.

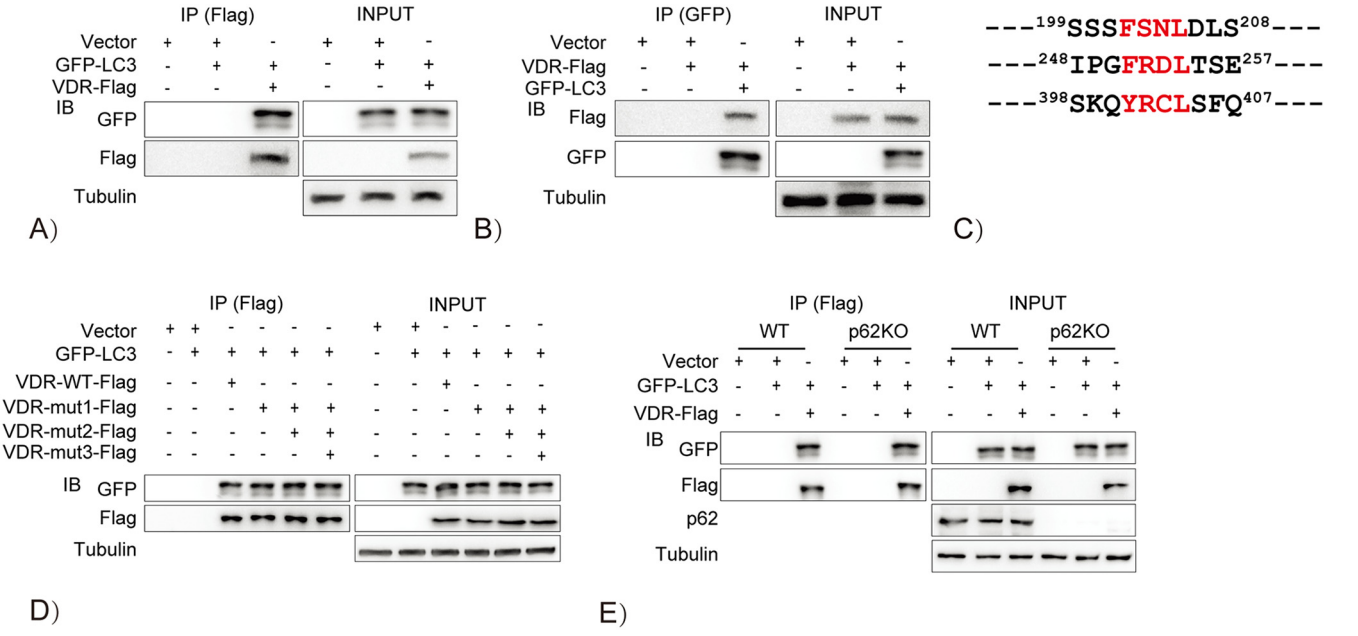

Fig. 3. VDR interacts with LC3. (A) Cell lysates (INPUT) and Flag-tagged immunoprecipitates (IP) of HEK293 cells transfected with the indicated plasmid in expression vectors were analyzed by immunoblotting (IB). (B) Cell lysates (INPUT) and GFP-tagged IP of HEK293 cells transfected with the indicated plasmid in expression vectors were analyzed by IB. (C) Schematic representation of LC3-interacting region (LIR) motifs in VDR sequence. (D) Cell lysates (INPUT) and Flag-tagged IP of HEK293 cells transfected with GFP-LC3 and/or different mutations of the VDR sequence were analyzed by IB. (E) Cell lysates (INPUT) and Flag-tagged IP of HEK293 wild-type (WT) cells and HEK293 p62 knockout (KO) cells transfected with the indicated plasmid in expression vectors were analyzed by IB. mutation 1: FRDL (TTCAGAGACCTC → AACAGAGACAAC); mutation 2: mutation1 + YRCL (ACCGCTGCCTC → GGCCGCTGCAAC); mutation 3: mutation2 + FSNL (TTCTCCAATCTG → GCCTCCAATGCG). Tubulin was used as the loading control.

the nucleus and lower in the cytoplasm than that in control cells (Fig. 2C–D). Next, we investigated the effect of LC3 on VDR transcription. As Fig. S2 showed, neither knockdown of LC3 nor overexpression of LC3 regulated the expression of VDR (Fig. S2). From these results, we hypothesized that LC3 regulates VDR via nuclear translocation instead of inducing its expression. Vitamin D, as the ligand of VDR, also promotes the nuclear translocation of the VDR. We found that paricalcitol (an activated vitamin D analog, pari) promoted the nuclear translocation of VDR in the absence of LC3, suggesting this effect was LC3-independent (Fig. S3).

3.3. LC3 interacts with VDR

To determine how LC3 promotes the nuclear translocation of VDR, co-IP was performed to examine whether LC3 interacted with VDR. HEK293 cells were transfected with GFP-tagged LC3 and Flag-tagged VDR or with the corresponding controls and examined with Flag-tagged IP. The results showed interaction between LC3 and VDR (Fig. 3A). Conversely, with GFP-tagged IP, the interaction was also seen (Fig. 3B). LC3-interacting proteins contain a short linear LC3-interacting region (LIR) motif, which is responsible for their interaction with LC3-family proteins [20]. The known consensus sequence for the core LIR motif is W/F/Y-x-x-L/I/V [21]. Therefore, we examined VDR sequence in silico and found that VDR possesses three putative LIR motifs (201FSNL206, 250FRDL255, and 400YRCL405) (Fig. 3C). Subsequently, we mutated the possible LIR motifs in VDR sequence (mutation 1: FRDL (TTCAGAGACCTC → AACA GAGACAAC); mutation 2: mutation1 + YRCL (ACCGCTGCCTC → GGCC GCTGCAAC); and mutation 3: mutation2 + FSNL (TTCTCCAATCTG → GCCTCCAATGCG)). Surprisingly, none of the mutations abolished the binding of VDR to LC3 (Fig. 3D), which indicated that LC3 might not bind to the VDR through the putative LIR motifs. During autophagy, LC3 interacts directly with p62 and recruits p62 into autophagosomes [22]. Moreover, p62 has been reported to interact directly with VDR and RXR [23]. To exclude p62-mediated interaction between LC3 and VDR, co-IP

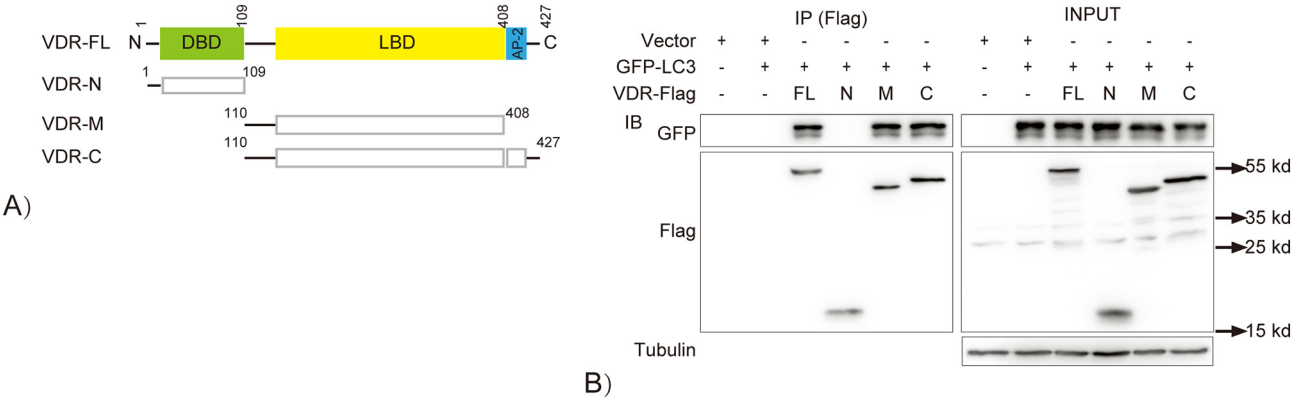

Fig. 4. Mapping of VDR interaction with LC3. (A) Schematic representation of the VDR domain structure. (B) Cell lysates (INPUT) and Flag-tagged immunoprecipitation (IP) of HEK293 cells transfected with GFP-LC3 and/or different VDR domains were analyzed by immunoblotting (IB). Tubulin was used as the loading control.

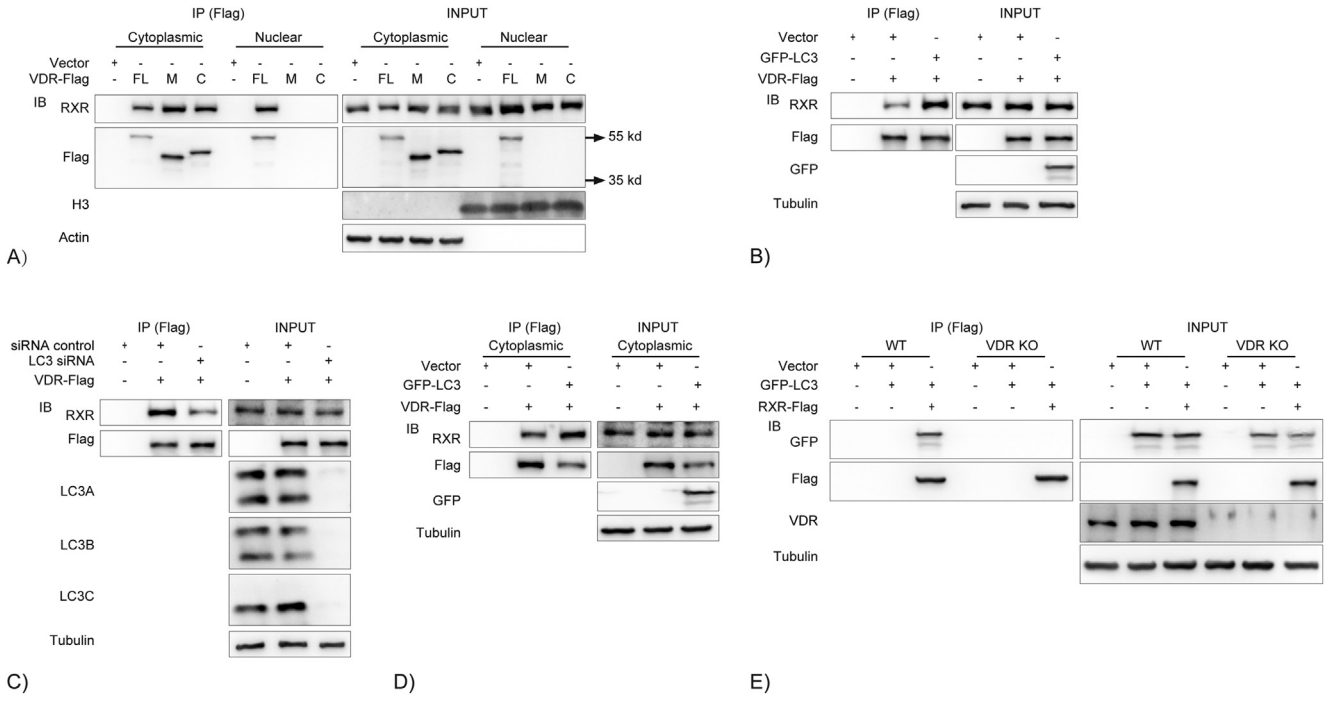

Fig. 5. LC3 promotes the heterodimerization of VDR with RXRα. (A) Cell cytoplasmic and nuclear lysates (INPUT) and Flag-tagged immunoprecipitation (IP) of HEK293 cells transfected with different VDR domains or corresponding controls were analyzed by immunoblotting (IB). Actin was used as the internal control for the cytoplasmic portion. H3 was used as the internal control for the nuclear portion. (B) Cell lysates (INPUT) and Flag-tagged immunoprecipitates (IP) of HEK293 cells transfected with VDR-Flag and GFP-LC3 or corresponding controls were analyzed by immunoblotting (IB). (C) Cell lysates (INPUT) and Flag-tagged immunoprecipitates of HEK293 cells transfected with VDR-Flag with/without LC3 siRNA were analyzed by IB. (D) Cell cytoplasmic lysates (INPUT) and Flag-tagged immunoprecipitates (IP) of HEK293 cells transfected with VDR-Flag and GFP-LC3 or corresponding controls were analyzed by immunoblotting (IB). (E) Cell lysates (INPUT) and Flag-tagged immunoprecipitates (IP) of HK-2 WT and VDR KO cells transfected with RXR-Flag and GFP-LC3 or corresponding controls were analyzed by immunoblotting (IB).Tubulin was used as the loading control.

was performed in p62-null HEK293 cells. The results showed that the interaction between LC3 and VDR was independent of p62 (Fig. 3E).

3.4. Identification of the LC3-interacting domain of VDR

Subsequently, we mapped the region(s) of VDR responsible for its interaction with LC3. HEK293 cells were transfected with different Flag-tagged VDR domains, GFP-tagged LC3, or the corresponding control vectors. The results showed that the interaction of VDR and LC3 was abrogated in cells expressing only the N-terminal region of the VDR (VDR—N), encompassing amino acids 1–109, establishing that VDR interacts with LC3 through the VDR ligand-binding domain (LBD), which encompasses amino acids 110–408 (VDR-M or VDR—C) (Fig. 4). Pari is VDR ligand that binds to its LBD domain, so we test if pari interferes the binding of LC3 and VDR. The result showed after pari treatment, the binding of LC3 and VDR was decreased (Fig. S4). This decrease perhaps due to both LC3 and pari interact with VDR through the same LBD domain, but its mechanism needs further study.

3.5. LC3 promotes the heterodimerization of VDR with RXRα

VDR functions as an obligate heterodimer in complex with RXRα [24], and our results showed that RXR can interact with VDR in both cytoplasm and nucleus. However, RXR only interact with VDR-M and VDR-C in cytoplasm because these two constructs cannot enter the nucleus without ligands [25] (Fig. 5A). We demonstrated earlier that LC3 can promote the nuclear translocation of VDR. To investigate the potential role of LC3 in the formation of the VDR:RXR heterodimer, we transfected HEK293 cells with VDR and either LC3 or vector and assessed VDR:RXR dimerization. The interaction between VDR and RXR was increased when LC3 was overexpressed (Fig. 5B) but decreased when LC3 was silenced (Fig. 5C). Then we demonstrated LC3 can promote the binding of VDR and RXR in cytoplasm as well (Fig. 5D). This pattern indicated that LC3 supports the formation of the VDR:RXR heterodimer. Next, the relationship between LC3 and RXR was examined, co-IP showed LC3 can interact with RXR, but the binding was abrogated in VDR KO cells (Fig. 5E), suggesting the binding of RXR and LC3 was VDR-dependent.

3.6. LC3 regulates the expression of fibrotic genes in HK-2 cells treated with HG via promoting VDR nuclear translocation

We demonstrated that LC3 regulates the nuclear translocation of VDR. Then, we investigated the potential role of LC3 in HK-2 cells treated with HG. As Fig. 6A shown, LC3 didn't regulate the expression of VDR. Compared with LG treatment, HG treatment can promote the

Fig. 6. LC3 regulates the expression of fibrotic genes in HK-2 cells treated with HG via promoting VDR nuclear translocation. (A) Western blot analysis of VDR protein levels at 48 h post high glucose treatment and transfection with pEGFP-C1 or GFP-LC3. Tubulin was used as the loading control. (B) Western blot analysis of cytoplasmic and nuclear VDR protein levels at 48 h post high glucose treatment and transfection with pEGFP or GFP-LC3. Actin was used as the internal control for the cytoplasmic portion. H3 was used as the internal control for the nuclear portion. (C) Immunofluorescence staining of the VDR (red) in cells treated with high glucose (HG) for 24 h after pEGFP-C1 or GFP-LC3 (green) overexpression is shown. DAPI (blue) was used to stain nuclei. At least 10 microscopic fields were assessed in each experiment. The images are representative of three independent experiments. Scale bar, 10 μm. The white arrow indicates the recovery of nuclear VDR. Ratios of positive cells (VDR nuclear translocation) among pEGFP-C1- or GFP-LC3-transfected cells were shown. $^{*}P < 0.05$. (D) Real-time quantitative PCR analysis of the COL1A1 and CTGF mRNA expression levels in HK-2 cells post high-glucose treatment and transfection with different VDR domains (VDR-FL, VDR-M and VDR—C). n = 3. NS: no significant. $^{**}P < 0.01$. (E) Real-time quantitative PCR analysis of the COL1A1 and CTGF mRNA expression levels in HK-2 cells and HK-2 VDR KO cells post high-glucose treatment and transfection with pEGFP-C1 or GFP-LC3. n = 3. NS: no significant. $^{**}P < 0.01$.

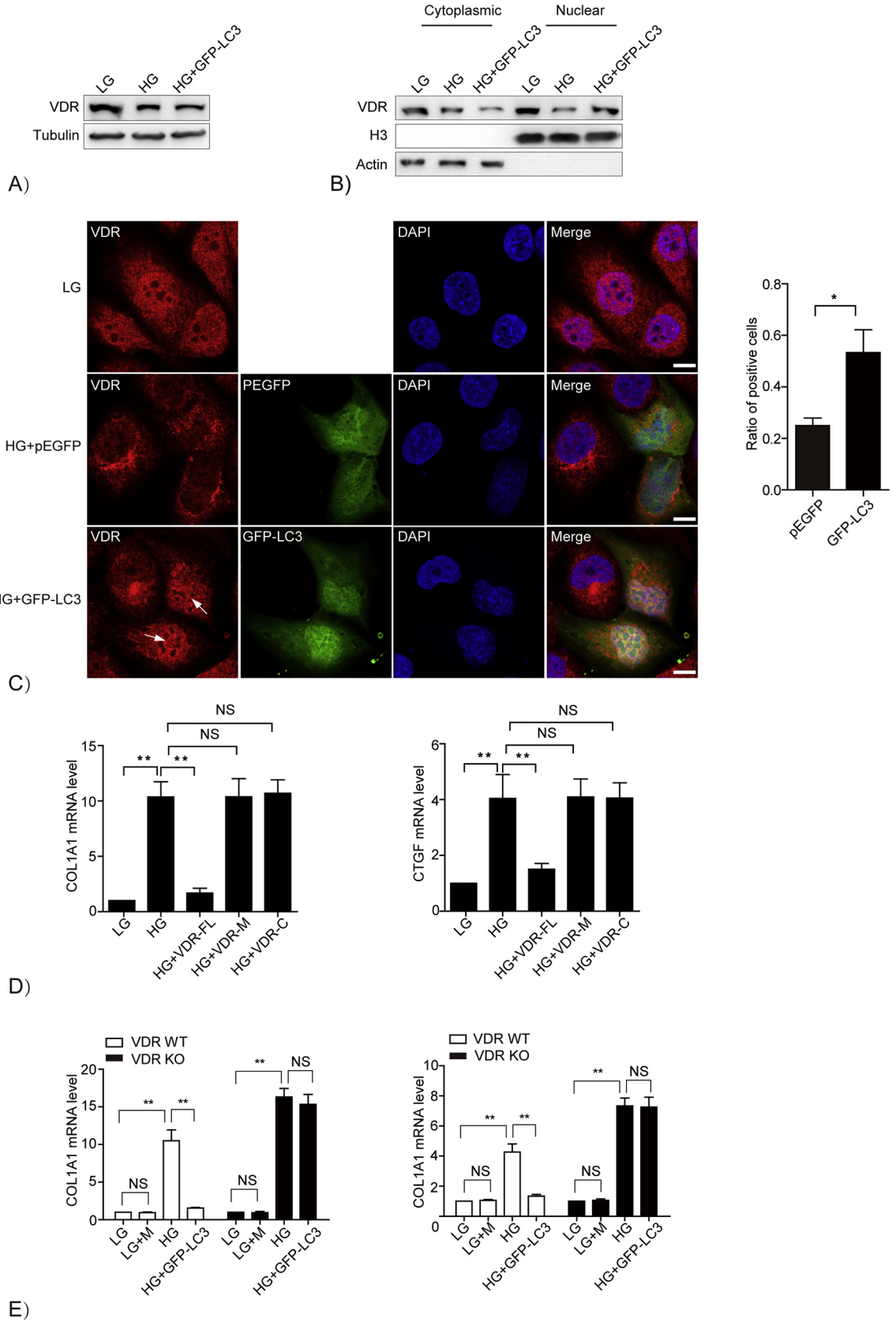
A)
LG
HG
HG+GFP-LC3
VDR
Tubulin
B)
Cytoplasmic
Nuclear
LG
HG
HG+GFP-LC3
LG
HG
HG+GFP-LC3
VDR
H3
Actin
C)
LG
HG+pEGFP
HG+GFP-LC3
VDR
DAPI
Merge
PEGFP
GFP-LC3
Ratio of positive cells
pEGFP
GFP-LC3
D)
COL1A1 mRNA level
CTGF mRNA level
NS
**
LG
HG
HG+VDR-FL
HG+VDR-M
HG+VDR-C
E)
VDR WT
VDR KO
COL1A1 mRNA level
LG
LG+M
HG
HG+GFP-LC3

translocation of nuclear VDR to the cytoplasm. However, HG-suppressed VDR nuclear distribution was partially recovered by the co-overexpression of LC3 (Fig. 6B–C). To explore the biological significance of LC3-mediated regulation of VDR distribution, VDR target genes involved in fibrosis of DN were analyzed. First, we treated HK-2 cells with high-glucose and transfected with different VDR domains (VDR-FL, VDR-M and VDR—C). As expected, the increased expression of COL1A1 and CTGF induced by HG was abolished by ectopic expression of VDR-FL, but not VDR-M or VDR-C (Fig. 6D). Interestingly, we showed that LC3 overexpression could also reverse HG-induced COL1A1 and CTGF level increase (Fig. 6E), indicating possible antifibrotic effect of LC3. We further employed VDR KO cells to investigate whether such effect of LC3 was mediated by VDR. We found that the expression of COL1A1 and CTGF was higher in VDR KO cells than in wild-type (WT) HK-2 cells (Fig. 6E), consistent with the published data in mice [6]. Moreover, the expression of fibrotic genes suppressed by ectopic LC3 in the presence of HG was completely abrogated in VDR KO cells (Fig. 6E).

4. Discussion

VDR is a member of the nuclear receptor superfamily [26]. Our previous study showed that VDR expression was downregulated in peripheral blood mononuclear cells (PBMCs) and renal tubular epithelial cells from type 2 DN patients [4]. The most well-known function of VDR is maintaining calcium and phosphorus homeostasis; however, accumulating evidence has demonstrated that VDRs perform renoprotective functions via their regulatory role in pathways associated with the inhibition of profibrotic growth factors and inflammatory cytokines and the suppression of the RAS [27–30]. VDR transcription depends on $1,25(OH)_2D_3$. After binding to $1,25(OH)_2D_3$, VDR forms a heterodimer with the RXR and enters the nucleus to modulate the expression of target genes [3]. However, the means by which VDR enters the nucleus still incompletely understood. We found that LC3 supports the formation of the VDR:RXR heterodimer and promotes the nuclear translocation of VDR, thus inhibiting profibrotic gene expression in HG-treated HK-2 cells by binding to the VDR.

LC3, a mammalian ortholog of yeast Atg8, is a key protein contributing to major steps in autophagy. Studies have verified that LC3-binding proteins contain a short hydrophobic LIR, more commonly referred to in yeast as the Atg8-interacting motif (AIM). Several autophagy receptors such as p62, BNIP3, BNIP3L, FUNDC1, NBR1, NDP52, and optineurin can interact simultaneously with autophagosomes through an interaction of their LIR motif with LC3 [31]. The interaction between p62 and LC3 via the LIR motif is necessary for autophagic degradation of p62-positive bodies containing ubiquitinated proteins [31]. Although Bnip3 is sufficient to induce the general autophagy response via its BH3 domain [32], inducing autophagic degradation of mitochondria (mitophagy) and the endoplasmic reticulum (ERphagy) requires the interaction of its LIR with Atg8 proteins [33]. However, research has determined that interaction with Atg8 family members does not necessarily require an LIR sequence. Behrends et al. found that a substantial portion of LC3-interacting proteins binds to LC3B in an LIR docking site-independent manner [34]. Studies have demonstrated that LC3 has functions other than mediating autophagy. LC3 is a microtubule-associated protein [9] and an interacting protein of the dendritic-specific Ca^{2+}-sensing protein [10]. Moreover, it regulates the level of fibronectin mRNA [11,12] and contributes to the negative regulation of SOS1-dependent Rac1 activation of membrane ruffling through interacting with SOS1, a guanine nucleotide exchange factor [13]. We found that the VDR can bind LC3 via its LBD domain in an LIR-independent manner.

VDR is a transcription factor that needs to be localized in nuclei to exert most of its function. Research has reported that importin 4 can promote the nuclear translocation of the VDR in a ligand-independent manner as a VDR-interacting protein [25] and, further, that CAN/Nup214, a component of the nuclear pore complex, can interact with the VDR and modulate its transcription factor activity [35]. However, the molecular mechanisms underlying the nuclear translocation of the VDR in a HG environment are unclear. We found that the levels of both nuclear VDR and LC3 are decreased in a HG environment but that overexpressed LC3 restores the nuclear VDR level, suggesting that HG may inhibit the nuclear translocation of the VDR through decreasing the level of nuclear LC3. LC3 is abundant in the nucleus, but its functions in autophagy are primarily conducted in the cytoplasm. Mechanisms underlying the nucleocytoplasmic shuttling of LC3 have been proposed, and studies have indicated that the nucleocytoplasmic distribution of LC3 is subject to regulation by protein-protein interactions in the cytoplasm [36,37]. Research by Rui Huang et al found that under nutrient deprivation conditions, nuclear LC3 was deacetylated by sirt1 and redistributed from the nucleus to the cytoplasm, while acetylation led to the transport of LC3 back to the nucleus [14]. Chen et al have demonstrated the nuclear import of LC3 was in a way dependent on importin-α/β [38], and VDR associated with importin α and mediated nuclear import of the VDR:RXR heterodimer [39], whether importin and LC3 cooperative in VDR's nuclear localization needs further study. Meanwhile, the mechanism by which HG reduces the expression of nuclear LC3 is not clear, and whether epigenetic modifications or protein-to-protein interactions are involved needs further study.

In conclusion, we demonstrated that LC3 is transported to the nucleus as a VDR-interacting protein and inhibits the HG-induced expression of fibrotic genes in HK-2 cells by promoting the formation of the VDR-RXR dimer.

Authors' contributions

Aimei Li and Hailong Han contributed to the testing, data analysis and interpretation. Aimei Li wrote the first draft of the manuscript. Bin Yi, Jieqiong Tan and Hao Zhang contributed to the study design and manuscript revision. Wei Zhang, Shikun Yang and Zhijun Huang were involved in specimen collection and the induction of the diabetic model. All authors read and approved the final manuscript.

Declaration of Competing Interest

None. The results presented in this paper have not been published previously and are not under consideration for publication elsewhere.

Acknowledgments

We would like to thank all of the patients for their participation in this study.

Funding

This study was funded by the New Xiangya Talent Project of Third Xiangya Hospital of Central South University (NO. 20160309). The sponsor had no influence on or participation in the preparation of this manuscript.

Appendix A. Supplementary data

Supplementary data to this article can be found online at https://doi.org/10.1016/j.metabol.2019.06.008.

References

[1] Afkarian M, Sachs MC, Kestenbaum B, Hirsch IB, Tuttle KR, Himmelfarb J, et al. Kidney disease and increased mortality risk in type 2 diabetes. J Am Soc Nephrol 2013; 24:302–8.
[2] Cooper ME. Pathogenesis, prevention, and treatment of diabetic nephropathy. Lancet 1998;352:213–9.

[3] Pike JW. Vitamin D3 receptors: structure and function in transcription. Annu Rev Nutr 1991;11:189–216.
[4] Yi B, Huang J, Zhang W, Li AM, Yang SK, Sun J, et al. Vitamin D receptor down-regulation is associated with severity of albuminuria in type 2 diabetes patients. J Clin Endocrinol Metab 2016;101:4395–404.
[5] Guo J, Lu C, Zhang F, Yu H, Zhou M, He M, et al. VDR activation reduces proteinuria and high-glucose-induced injury of kidneys and podocytes by regulating Wnt signaling pathway. Cell Physiol Biochem 2017;43:39–51.
[6] Zhang Y, Kong J, Deb DK, Chang A, Li YC. Vitamin D receptor attenuates renal fibrosis by suppressing the renin-angiotensin system. J Am Soc Nephrol 2010;21:966–73.
[7] Nakatogawa H, Ishii J, Asai E, Ohsumi Y. Atg4 recycles inappropriately lipidated Atg8 to promote autophagosome biogenesis. Autophagy 2012;8:177–86.
[8] Weidberg H, Shvets E, Shpilka T, Shimron F, Shinder V, Elazar Z. LC3 and GATE-16/GABARAP subfamilies are both essential yet act differently in autophagosome biogenesis. EMBO J 2010;29:1792–802.
[9] Mann SS, Hammarback JA. Molecular characterization of light chain 3. A microtubule binding subunit of MAP1A and MAP1B. J Biol Chem 1994;269:11492–7.
[10] Seidenbecher CI, Landwehr M, Smalla KH, Kreutz M, Dieterich DC, Zuschratter W, et al. Caldendrin but not calmodulin binds to light chain 3 of MAP1A/B: an association with the microtubule cytoskeleton highlighting exclusive binding partners for neuronal Ca(2+)-sensor proteins. J Mol Biol 2004;336:957–70.
[11] Zhou B, Rabinovitch M. Microtubule involvement in translational regulation of fibronectin expression by light chain 3 of microtubule-associated protein 1 in vascular smooth muscle cells. Circ Res 1998;83:481–9.
[12] Zhou B, Boudreau N, Coulber C, Hammarback J, Rabinovitch M. Microtubule-associated protein 1 light chain 3 is a fibronectin mRNA-binding protein linked to mRNA translation in lamb vascular smooth muscle cells. J Clin Invest 1997;100:3070–82.
[13] Furuta S, Miura K, Copeland T, Shang WH, Oshima A, Kamata T. Light Chain 3 associates with a Sos1 guanine nucleotide exchange factor: its significance in the Sos1-mediated Rac1 signaling leading to membrane ruffling. Oncogene 2002;21:7060–6.
[14] Huang R, Xu Y, Wan W, Shou X, Qian J, You Z, et al. Deacetylation of nuclear LC3 drives autophagy initiation under starvation. Mol Cell 2015;57:456–66.
[15] Zhong F, Chen H, Xie Y, Azeloglu EU, Wei C, Zhang W, et al. Protein S protects against podocyte injury in diabetic nephropathy. J Am Soc Nephrol 2018;29:1397–410.
[16] Stieger N, Worthmann K, Teng B, Engeli S, Das AM, Haller H, et al. Impact of high glucose and transforming growth factor-beta on bioenergetic profiles in podocytes. Metabolism 2012;61:1073–86.
[17] Koukourakis MI, Kalamida D, Giatromanolaki A, Zois CE, Sivridis E, Pouliliou S, et al. Autophagosome proteins LC3A, LC3B and LC3C have distinct subcellular distribution kinetics and expression in cancer cell lines. PLoS One 2015;10:e0137675.
[18] Madjo U, Leymarie O, Fremont S, Kuster A, Nehlich M, Gallois-Montbrun S, et al. LC3C contributes to Vpu-mediated antagonism of BST2/Tetherin restriction on HIV-1 release through a non-canonical autophagy pathway. Cell Rep 2016;17:2221–33.
[19] Zhang H, Li A, Zhang W, Huang Z, Wang J, Yi B. High glucose-induced cytoplasmic translocation of Dnmt3a contributes to CTGF hypo-methylation in mesangial cells. Biosci Rep 2016;36.
[20] Birgisdottir AB, Lamark T, Johansen T. The LIR motif - crucial for selective autophagy. J Cell Sci 2013;126:3237–47.
[21] Johansen T, Lamark T. Selective autophagy mediated by autophagic adapter proteins. Autophagy 2011;7:279–96.
[22] Shvets E, Fass E, Scherz-Shouval R, Elazar Z. The N-terminus and Phe52 residue of LC3 recruit p62/SQSTM1 into autophagosomes. J Cell Sci 2008;121:2685–95.
[23] Duran A, Hernandez ED, Reina-Campos M, Castilla EA, Subramaniam S, Raghunandan S, et al. p62/SQSTM1 by binding to vitamin D receptor inhibits hepatic stellate cell activity, fibrosis, and liver cancer. Cancer Cell 2016;30:595–609.
[24] Shaffer PL, Gewirth DT. Structural basis of VDR-DNA interactions on direct repeat response elements. EMBO J 2002;21:2242–52.
[25] Miyauchi Y, Michigami T, Sakaguchi N, Sekimoto T, Yoneda Y, Pike JW, et al. Importin 4 is responsible for ligand-independent nuclear translocation of vitamin D receptor. J Biol Chem 2005;280:40901–8.
[26] Haussler MR, Whitfield GK, Haussler CA, Hsieh JC, Thompson PD, Selznick SH, et al. The nuclear vitamin D receptor: biological and molecular regulatory properties revealed. J Bone Miner Res 1998;13:325–49.
[27] Zhang Z, Yuan W, Sun L, Szeto FL, Wong KE, Li X, et al. 1,25-Dihydroxyvitamin D3 targeting of NF-kappaB suppresses high glucose-induced MCP-1 expression in mesangial cells. Kidney Int 2007;72:193–201.
[28] Li YC, Kong J, Wei M, Chen ZF, Liu SQ, Cao LP. 1,25-Dihydroxyvitamin D(3) is a negative endocrine regulator of the renin-angiotensin system. J Clin Invest 2002;110:229–38.
[29] Meems LM, Cannon MV, Mahmud H, Voors AA, van Gilst WH, Sillje HH, et al. The vitamin D receptor activator paricalcitol prevents fibrosis and diastolic dysfunction in a murine model of pressure overload. J Steroid Biochem Mol Biol 2012;132:282–9.
[30] Yang S, Li A, Wang J, Liu J, Han Y, Zhang W, et al. Vitamin D receptor: a novel therapeutic target for kidney diseases. Curr Med Chem 2018;25:3256–71.
[31] Pankiv S, Clausen TH, Lamark T, Brech A, Bruun JA, Outzen H, et al. p62/SQSTM1 binds directly to Atg8/LC3 to facilitate degradation of ubiquitinated protein aggregates by autophagy. J Biol Chem 2007;282:24131–45.
[32] Bellot G, Garcia-Medina R, Gounon P, Chiche J, Roux D, Pouyssegur J, et al. Hypoxia-induced autophagy is mediated through hypoxia-inducible factor induction of BNIP3 and BNIP3L via their BH3 domains. Mol Cell Biol 2009;29:2570–81.
[33] Hanna RA, Quinsay MN, Orogo AM, Giang K, Rikka S, Gustafsson AB. Microtubule-associated protein 1 light chain 3 (LC3) interacts with Bnip3 protein to selectively remove endoplasmic reticulum and mitochondria via autophagy. J Biol Chem 2012;287:19094–104.
[34] Behrends C, Sowa ME, Gygi SP, Harper JW. Network organization of the human autophagy system. Nature 2010;466:68–76.
[35] Miyauchi Y, Sakaguchi N, Okada T, Makishima M, Ozono K, Michigami T. Oncogenic nucleoporin CAN/Nup214 interacts with vitamin D receptor and modulates its function. J Cell Biochem 2009;106:1090–101.
[36] Fujita N, Hayashi-Nishino M, Fukumoto H, Omori H, Yamamoto A, Noda T, et al. An Atg4B mutant hampers the lipidation of LC3 paralogues and causes defects in autophagosome closure. Mol Biol Cell 2008;19:4651–9.
[37] Drake KR, Kang M, Kenworthy AK. Nucleocytoplasmic distribution and dynamics of the autophagosome marker EGFP-LC3. PLoS One 2010;5:e9806.
[38] Chen GY, Meng CL, Lin KC, Tuan HY, Yang HJ, Chen CL, et al. Graphene oxide as a chemosensitizer: diverted autophagic flux, enhanced nuclear import, elevated necrosis and improved antitumor effects. Biomaterials 2015;40:12–22.
[39] Yasmin R, Williams RM, Xu M, Noy N. Nuclear import of the retinoid X receptor, the vitamin D receptor, and their mutual heterodimer. J Biol Chem 2005;280:40152–60.